analytica

MDPI

Article

Dose–Response Curve in REMA Test: Determination from Smartphone-Based Pictures

Eugene B. Postnikov [1], Alexander V. Sychev [2] and Anastasia I. Lavrova [3,4,*]

[1] Department of Theoretical Physics, Kursk State University, Radishcheva st. 33, Kursk 305000, Russia; postnikov@kursksu.ru
[2] Research Center for Condensed Matter Physics, Kursk State University, Radishcheva st. 33, Kursk 305000, Russia; sychev_av@kursksu.ru
[3] Saint-Petersburg State Research Institute of Phthisiopulmonology, Lygovsky av. 2–4, Saint-Petersburg 191036, Russia
[4] Sophya Kovalevskaya North-West Mathematical Research Center, Immanuel Kant Baltic Federal University, Nevskogo St. 14, Kaliningrad 236041, Russia
* Correspondence: aurebours@googlemail.com

Abstract: We report a workflow and a software description for digital image colorimetry aimed at obtaining a quantitative dose–response curve and the minimal inhibitory concentration in the Resazurin Microtiter Assay (REMA) test of the activity of antimycobacterial drugs. The principle of this analysis is based on the newly established correspondence between the intensity of the a^* channel of the CIE L*a*b* colour space and the concentration of resorufin produced in the course of this test. The whole procedure can be carried out using free software. It has sufficiently mild requirements for the quality of colour images, which can be taken by a typical smartphone camera. Thus, the approach does not impose additional costs on the medical examination points and is widely accessible. Its efficiency is verified by applying it to the case of two representatives of substituted 2-(quinolin-4-yl) imidazolines. The direct comparison with the data on the indicator's fluorescence obtained using a commercial microplate reader argues that the proposed approach provides results of the same range of accuracy on the quantitative level. As a result, it would be possible to apply the strategy not only for new low-cost studies but also for expanding databases on drug candidates by quantitatively reprocessing existing data, which were earlier documented by images of microplates but analysed only qualitatively.

Keywords: REMA; resazurin; resorufin; microbiological analysis; digital image colorimetry; minimal inhibitory concentration

Citation: Postnikov, E.B.; Sychev, A.V.; Lavrova, A.I. Dose–Response Curve in REMA Test: Determination from Smartphone-Based Pictures. *Analytica* **2024**, *5*, 619–631. https://doi.org/10.3390/analytica5040041

Academic Editors: Marcello Locatelli and Halil Ibrahim Ulusoy

Received: 30 September 2024
Revised: 28 November 2024
Accepted: 5 December 2024
Published: 10 December 2024

1. Introduction

Recently, digital image colorimetry based on images taken by modern smartphones has gained drastically growing attention as a method of quantitative chemical and biochemical analysis [1,2]. Modern devices allow for obtaining high-quality images with rich colour resolution, which makes it possible to obtain not only qualitative differences in the indicator medium responding to the content of substances subjected to analysis but even quantitative spectral information. This allows for the development of low-cost and widespread analytical laboratory devices [3]. Colorimetric biomedical applications include controlling sweat and salivary pH accompanying physical activity [4], immunoassays [5], biochemical analysis of serum analytes [6], glucose [7] and haemoglobin [8] level monitoring, and many others.

Also, a smartphone can be incorporated into portable photometric devices as the registering block. After being supplied with a data processing application, it has been shown that such a construction can determine quantitative responses to the growth of microorganisms in microplates. Devices include, among others, a portable instrument that

supports colorimetric, fluorescence, luminescence, and turbidity analyses with various reagents [9], as well as a device utilising microplates made from indicator paper containing resazurin, which responds to bacterial metabolic activity [10]. From the colorimetric point of view, both approaches control the values of hue in the HSL encodings of the RGB system.

At the same time, it is worth noting that smartphone-based approaches, which are reported as providing high-accuracy results, require ensuring special conditions for photo registration. These may include special black box chambers with controlled and specified illumination, or even incorporating smartphones as a block into specially assembled devices. However, many practical, routinely carried out assays include simple photographing of microplates just for documentation, without extra care regarding the illumination conditions. For example, they are also used for the qualitative determination of the minimal inhibitory concentration within the Resazurin Microtiter Assay (REMA), intended to determine the minimal inhibitory concentration (MIC) of antibiotics acting on a culture of *M. tuberculosis*. This test is based on the ability of the blue nonfluorescent indicator, resazurin, to be reduced into the pink fluorescent resorufin [11]. Recently, it has been one of the standard methods of testing the drug sensibility of different *Mycobacterium* species and strains [12–14]. However, in the conventional approach, one needs only to determine the maximal dilution of a drug, which does not lead to a visible change of colour.

More quantitative assays utilise the fluorescence of resorufin for the obtaining and analysis of drug–response curves [15–17]. But spectrophotometric plate readers are bulky and expensive devices in contrast to widespread and low-cost smartphones. Thus, a curious question is whether it is possible to use typical photos for the quantitative acquisition of the dose–response curves characterising the outputs of the REMA procedure.

There are a number of works in which such a problem was attempted but, in their majority, the RGB colour scheme, native to digital pictures, has been used. In the study [18], the authors established a correlation between specially weighted combinations of values from the red and green channels of CCD camera images and the concentrations of resorufin. These concentrations were determined using a spectrophotometric microplate reader, based on absorbance data measured at 595 nm and 490 nm.

The correlation of the values in the red channel and the level of resazurin's fluorescence was demonstrated in the work [19]. Authors of the work [20] demonstrated the application of smartphone-based image processing to evaluate tubes containing resazurin as an indicator of bacterial growth under the influence of antibiotics. They further highlighted that using the red channel in RGB colour images effectively reproduces the sigmoidal response of the logarithm of the concentration of the acting substance, consistent with the pharmacokinetic theory

But it should be stressed that the RGB colour scheme is significantly device-dependent and not perceptually uniform, i.e., numerical changes in its channels do not have direct proportionality to the light spectral content and perceived change in colour [21]. From this point of view, the colour space CIE L*a*b* developed by the International Commission on Illumination (CIE), which is device-independent, based on spectral mapping functions and treating the colour difference as the Euclidean distance between colour coordinates (this means that there is an explicit quantitative measure for the difference between two colours in contrast to the RGB system), looks more preferable [22]. It is also worth noting that the colour space CIE L*a*b* explicitly distinguishes between luminosity (the channel L*) and the chromatic colour specification (the pair (a*,b*)). This compensates for possible variations in the brightness of images of solutions in different wells of the microplate, but in the RGB colour space, they valuably affect all colour channels.

Recently, we have shown [23] that for the colour change typical for the REMA test with the standard laboratory strain of *M. tuberculosis*, it is possible to establish a quantitative correlation between resorufin concentrations and values of the a* channel that correspond to the transition from blue to red colour. It remains unexplored whether the relationship between colour channel values and the concentration of antibacterial drugs can quantitatively match the fluorometric dose–response curve, a key characteristic used to

evaluate the efficacy of therapeutic agents. This question is particularly relevant in the case of drug-resistant mycobacterial strains, where standard methodologies may fall short in accurately assessing treatment efficacy [24].

Thus, the purpose of this work consists of two main goals: (i) establishing the correspondence between the dose–response curves obtained from the colorimetric analysis of a microbiological plate's image taken with a smartphone; (ii) developing a computer program intended to be used for such analysis in practical applications. Special attention will be paid to the use of open-source software, as this approach, combined with the use of widely available smartphones for image capture, would significantly enhance the accessibility of the method. This would allow for broader application beyond laboratories equipped with costly commercial equipment and proprietary software, making it a more viable option for resource-limited settings.

2. Materials and Methods

2.1. Data Used for the Approach's Testing

To explore the validity of the proposed method and software, we use the data reported in the work [25] as open-source data of two types. The Supplementary Material to this article contains the data characterising the action on *M. tuberculosis*, strain H37Rv, of two substances developed as possible candidates for antimycobacterial drugs: (1-4-[2-(Quinolin-4-yl)-4,5-dihydro-1H-imidazol-1-yl]pyrimi-din-2-ylpiperidin-4-yl)methanol (denoted as "compound 16" in the cited paper) and 4-1-[6-(Morpholin-4-yl)pyrazin-2-yl]-4,5-dihydro-1H-imidazol-2-ylquinoline (denoted as "compound 18"). The authors provided both colour pictures of microbiological plates taken by a smartphone after the REMA test and tables reporting the respective fluorescence level in each well of the plate recorded using a FLUOstarOptima (BMG Labtech, Offenburg, Germany) plate reader. The fluorometric data are reported there as tables containing the raw outputs of the plate reader. The smartphone-based images are incorporated in pdf files with size reduction. Thus, when extracted from the pdf file, they have the resolution 513 × 404 px and 550 × 452 px for compounds 16 and 18, respectively.

Note that the fluorometric data satisfy the generalised Hill function in response to the drug concentration, i.e., a well-supported pharmacokinetic model, which was shown in the work [26] earlier (the details of the fitting procedure can be found in the cited paper). Thus, this allows the direct comparison of conclusions based on the simultaneous processing of the conventional fluorometric and new colorimetric approaches. It is worth noting that the data are published under the free access option and, therefore, can be easily accessed to check the results of their processing within the procedure described below.

As a preliminary step, the images of microplates were extracted from pdf-formatted files as pictures and preprocessed using the image processing software ImageJ. Since the images under consideration were taken without a specially controlled illumination, the rolling ball algorithm [27] was applied to correct the non-uniformity of the background illumination (ImageJ's procedure 'Process/Subtract Background'; ImageJ v. 1.54i was used); the rolling ball's radii were equal to 50 and 30 pixels for compounds 16 and 18, respectively. The radii were chosen according to the method's specification, requiring their value to be comparable with the size of the largest objects of interest. In our case, these sizes are the diameters of the wells, which are about these numbers of pixels at the resolution of available pictures. As a result, the average intensity over the region covered by the ball was subtracted from the original image, leading to the correction of spatial variations in the background intensity.

As the following step, the 'PlateReader 3.0' plugin of ImageJ [28] was applied to extract information on the colour in individual wells of the plate. Since 'PlateReader 3.0' operates with the native RGB colour coding of the processed image, three output tables in the plugin's standard form were generated and saved to text files entitled 'Red.csv', 'Green.csv', and 'Blue.csv'. Additionally, a text file entitled 'Conc.csv' was created to contain values of the drug concentrations added to columns of the plate as well as for the control (0:

the mycobacterial culture without the drug (zero concentration); 'C1%': 1% initial dilution of the culture; and 'C': pure solution of resazurin without the bacterial culture). Folders with all these files are provided in the Supplementary Material.

2.2. Software Developed for Colorimetric Pharmacokinetic Analysis

The program developed for pharmacokinetic analysis is written as a program file entitled `ColorMICplate.m` (provided in the Supplementary Material; a manual commenting on the whole image processing procedure step by step and supplied with screenshots is also given there), which can be run using both the open source software Octave (with the preliminary loaded packages `image` and `optim`) and the commercial software MATLAB (with `Image Processing Toolbox` and `Optimization Toolbox`) and tested using Octave 9.2.0 and MATLAB R2014b.

The program is equipped with a simple graphic user interface (GUI), see Figure 1. At the start, the evoking message appears. It contains instructions to choose a folder, where the four required .csv files described above are located. Since the names of the files are standardised, it is advisable to keep data for each processed plate in a separate folder indicated by its name. In this case, the results of data processing will be kept in the same folder, providing a complete and reproducible set. After pressing 'OK', the GUI dialogue for the folder choice will be activated, and the data uploaded and initially processed using default settings. After this, the main window (see Figure 1) will be activated.

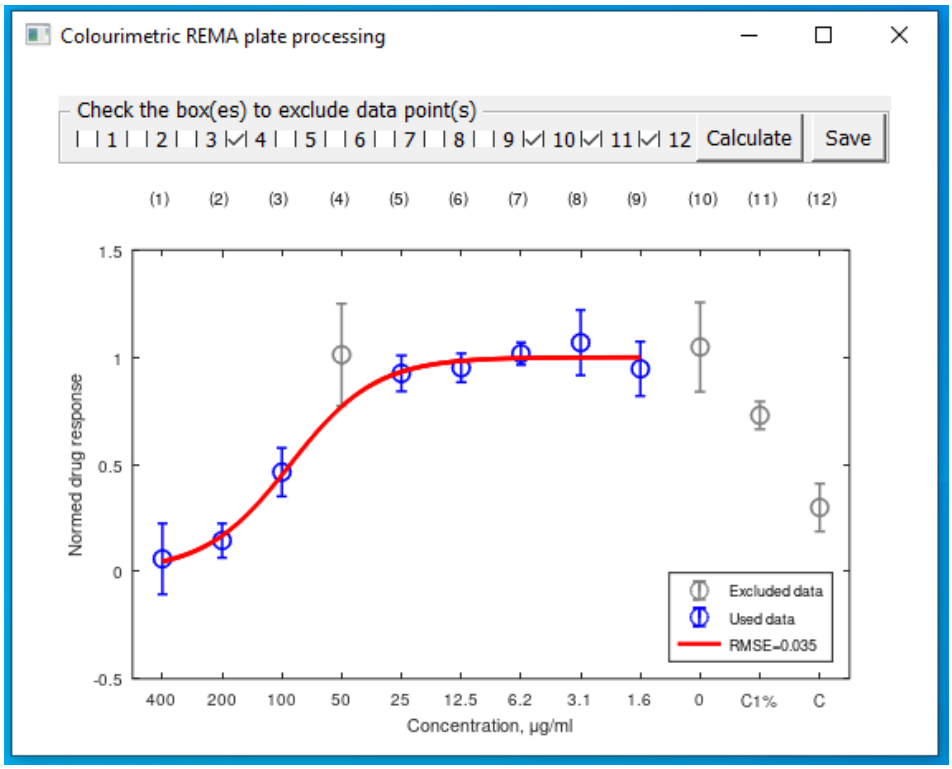

Figure 1. Main window of the developed program's graphic user interface. It demonstrates the graphic window displaying the normed drug–response curve and its regression according the notation in the input data files as well as the control panel, which allows to user to choose required data, run calculations, and save their result.

By default, a set of concentrations listed in the file 'Conc.csv' as numerical data will be read and used for the functional data fitting. A string of character values will be used only for the statistical data processing of colorimetric information and naming abscissa in the plot. For this reason, if one needs to use a mixed notation for some control columns (like 'C1%'), it must be started from a letter, not a number.

Note that the 'PlateReader 3.0' plugin implements the procedure of colour correction in each target circular area made, respectively, from the values within small circles surrounding the target well [28]. The obtained corrected data are placed in the output .csv files in the column entitled 'Acorr'. This values relates to the colour channel intensity I_{corr} (within the range from 0 to 1) as

$$I_{corr} = 10^{-Acorr} = \frac{I}{I_{surr}}. \tag{1}$$

Here, I is the mean value of pixels within the target area and I_{surr} is the same for surrounding small circles.

But in practice, it occurs that $I_{corr} > 1$ may appear when there is a glare on the photo. For this reason, an additional check is applied: we search for $Nrm = \max\{I^R_{corr}, I^G_{corr}, I^B_{corr}\}$ and the channel intensities are rescaled as $I_{corr} := I_{corr}/Nrm$ for all three channels if $Nrm > 1$. Otherwise, they remain as provided in the input files.

After this, the RGB triplets for all lines corresponding to the plate's wells are mapped to the CIE L*a*b* colour space and the one-dimensional array of values a corresponding to the channel a* are extracted. For each column containing the same drug concentration, the median value a_M and median average deviation (MAD) of data from it a_{mad} are determined by the standard routines. The choice of these characteristics is based on the small size of the set and unknown probabilistic properties (including a high probability of the presence of a few outliers) of individual measurements. In such cases, as noted in [29], median-based statistics are robust and therefore preferable. In Figure 1, the median values, represented by circles, are accompanied by whiskers, which denote the median absolute deviation (MAD) multiplied by 1.5. This factor is chosen because it closely approximates the ratio of the MAD to the standard deviation for normally distributed random variables.

The obtained median values corresponding to non-zero drug concentrations are fitted by the generalised four-parametric Hill function, which determines a standard dose–response curve [30]

$$a(c) = \beta_1 + \frac{\beta_2 - \beta_1}{1 + \left(\frac{c}{\beta_3}\right)^{\beta_4}}, \tag{2}$$

where β_1 and β_2 are lower and upper asymptotes (here in the units of the CIE L*a*b* colour scale) of the sigmoidal response functions (for infinite and zero concentrations, respectively), β_3 gives the concentration at which half of the possible response is achieved, and β_4 is the phenomenological Hill coefficient (but, in principle, related to biochemical binding processes). The program fulfils the procedure of fitting Equation (2) to the experimental data using the standard MATLAB/Octave function `nlinfit`, which realises the Levenberg–Marquardt nonlinear least squares algorithm.

For practical biomedical consideration, direct colorimetric units are not so informative. Hence, we use the rescaling

$$\tilde{a}_M = \frac{a_M - \beta_1}{\beta_2 - \beta_1}, \quad \tilde{a}_{mad} = \frac{a_{mad}}{\beta_2 - \beta_1}, \quad \tilde{a}(c) = \frac{a(c) - \beta_1}{\beta_2 - \beta_1}, \tag{3}$$

which gives the straightforward range of variation in the normed dose–response curve from 0 (there is no growth of the culture completely) to 1 (the growth of the culture is completely unaffected), with the following two-parametric formula:

$$\tilde{a}(c) = \left[1 + \left(\frac{c}{IC_{50}}\right)^{\alpha}\right]^{-1}, \tag{4}$$

where $IC_{50} = \beta_3$ is the 50% inhibitory concentration and $\alpha = \beta_4$ is Hill's index. The markers and curve in Figure 1 illustrate this representation.

At the first run, all data points corresponding to numerical concentrations are used for the fitting procedure, and the respective curve is plotted and supplied with a leg-

end containing the value of the Root Mean Square Error (RMSE) for the fit. Thus, one can (i) check whether the fitting curve goes through all data points within the limits of their uncertainty indicated by error bars; (ii) estimate the RMSE's numerical value with respect to the range of data uncertainties. Visually detected outliers, which violate condition (i), can be excluded manually using the check boxes placed on the upper side of the interface window. In addition, other suspicious points (e.g., with extremely high uncertainty levels) can be excluded; as the procedure can be repeated several times, after some variants of this procedure of point exclusion the minimisation of the RMSE can be achieved. In the program's main window, excluded points are denoted by grey colour. Note also that wells corresponding to the control (non-numerical subscripts and zero) are always excluded independently on the check box marker. An example of such a procedure is also illustrated in the program's manual, placed in the Supplementary Material.

Equation (4) also results in the explicit expression for concentrations corresponding to the qth percentile of growth inhibition

$$IC_q = IC_{50}\left(\frac{q}{100-q}\right)^{\frac{1}{\alpha}}. \quad (5)$$

When the optimal curve fitting is determined, pressing the button 'Save' exports the respective plot supplied with the list parameters of Equation (5), the resulting RMSD, and, additionally, IC_{75} and IC_{90}. After this, the user can return to fitting with the uploaded dataset, upload new data, or exit from the program.

3. Results

Figure 2A,B demonstrate the schemes of the average colour distribution among the wells of the microbiological plates, the source of which is described in Section 2.1.

With the developed program code, the values of the colour channel a* of the colour system CIE L*a*b* were extracted and are shown in Figure 2C,D as circles (in the normed representation). For the comparison, asterisks show the values of the fluorescence level reported in the work [25] (the same normalisation is applied). One can see that both types of markers follow the same trend and are located pairwise closely to each other. Quantitatively, the Mann–Whitney U-test indicates that these two sequences are equivalent, with a p-value equal to 0.742 for compound 16 and 0.896 for compound 18, even if all data from all columns from 1 to 11 are taken (the last column, 12, is excluded since there are no fluorescence data there).

As the next step, we processed these data, searching for the colorimetric dose–response curve parameters. In this case, columns 10–12, which do not correspond to definite positive concentrations of an acting substance, were excluded from the process of fitting. For compound 16, the datum corresponding to the concentration 50 μg/mL with a wide range of uncertainty was excluded too, since this exclusion optimises the MRSE. For compound 18, the first two data points corresponding to the concentrations 400 μg/mL and 200 μg/mL were excluded, since they do not follow a monotonic response to the dose change.

Data fitting with Equation (2) and subsequent rescaling to Equation (4) results in the curves shown by solid lines in Figure 2C,D. For comparison, the same procedure applied to the tables of fluorescence values reported (for the same set of concentrations) in the work [25] gives the dashed curves placed in the same subpanels of Figure 2. The parameters of these curves are provided in Table 1 as well as the values of three typical levels of inhibitory concentration, which follow from them using Equation (5).

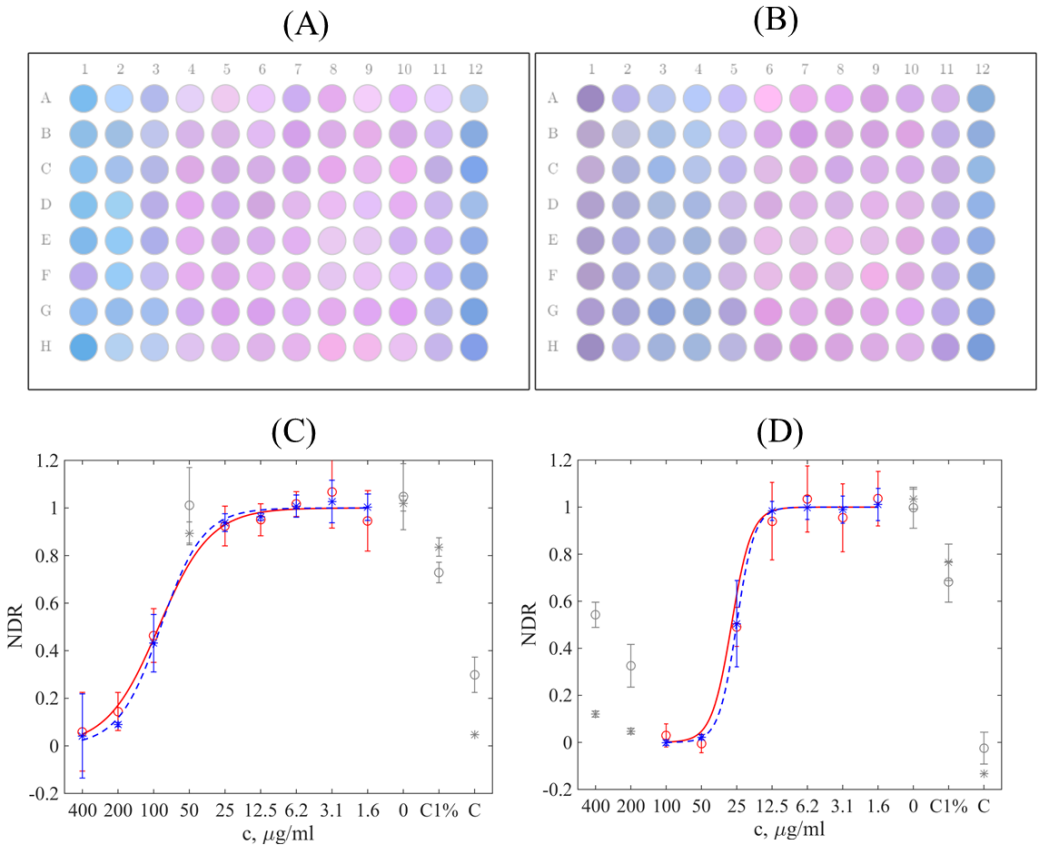

Figure 2. Distribution of extracted average colours over the plate wells in the REMA test results for the compounds 16 (**A**) and 18 (**B**); markers denote the normed responses in the a* channel of the CIE L*a*b* colour system (circles) and the fluorescence data (asterisks) for the compounds 16 (**C**) and 18 (**D**), with abscissa labelling according to the notation in the pictures of plates reported in the work [25], which includes not only drug concentrations but also control cells (0, *C*1% (1% control dilution of the bacterial culture), and *C* (the control representing medium without the bacterial culture), not used in the calculations). Coloured markers are used for the regression, grey ones are not. The red solid (colorimetric) and blue dashed (fluorometric) curves satisfy Equation (4), with parameters listed in Table 1.

The obtained parameters and characteristics of both (colorimetric and fluorometric) approaches do not exhibit a significant difference. Qualitatively, this is seen from the comparison of the size of whiskers, indicating the uncertainty of the data and the difference between the two fitting curves, which remains inside of the respective pathways. Quantitatively, we estimated the characteristic uncertainty range using the Monte Carlo approach. We formed an ensemble of 10^4 realisations with the Gaussian-distributed elements having the mean values $\tilde{a}_M$ and the standard deviation $\tilde{a}_{mad}$, refitted each realisation, and then carried out statistical analysis of the obtained coefficients and parameters. In particular, for compound 16, the interquartile range 0.32–0.68 corresponding to the standard uncertainty of IC_{75} is [87.9, 174] μg/mL, i.e., wider than the difference with the fluorescence-based parameter listed in Table 1. For compound 18, the situation is the same.

Table 1. Parameters of the normed dose–response curve (4) for the studied compounds obtained using colorimetric data processed with the proposed method and software and from the fluorometric data reported in the work [25].

Colorimetry					
Compound	α	$IC_{50}/(\mu g/mL)$	$IC_{75}/(\mu g/mL)$	$IC_{90}/(\mu g/mL)$	**RMSE**
16	2	90.6	156	267	0.035
18	5.1	24.7	30.7	38.1	0.032
Fluorescence					
Compound	α	$IC_{50}/(\mu g/mL)$	$IC_{75}/(\mu g/mL)$	$IC_{90}/(\mu g/mL)$	**RMSE**
16	2.4	87.2.6	137	215	0.020
18	5.7	25.1	30.4	36.9	0.006

4. Discussion

The widespread conventional definition of the visually determined minimal inhibitory concentration (MIC) operates with a discrete set concentrations used as sequential dilution sets. As a result, the MIC is defined [12] as the value of the lowest concentration of the drug preventing a colour change of resazurin added to the wells of the microbiological plate. At the same time, the practical application of this approach can be rather complicated: subpanels (A) and (B) in Figure 2A illustrate such a situation, where variations in colour and light intensity are significantly high, contrast is low, and a certain decision is questionable.

The application of the CIE L*a*b* colour space instead of the original RGB scheme provides an advantage in this case. One of the key properties of the CIE L*a*b* is that colour information (a* and b*) is separated from the illumination (L*). Therefore, the scattering of lightness of the picture does not affect the distribution of colour changes. Since the latter, typical for the transition between colours of resazurin and resorufin, is aligned with the colour variation along the a* axis, the obtained colorimetric curve corresponds to the change in resorufin's concentration. To illustrate this line of reasoning, in addition to the purely experimental correlations discussed in the work [23], we evaluated the computational model implemented using the 'ColorCalculator, v. 7.77' software (Osram Sylvania Inc., Beverly, MA, USA). To calculate the spectral filtration of illumination created by the standard illuminant D65 mimicking north sky daylight, the UV–vis spectra of both chemicals reported in the reference database [31,32] were used to reproduce the spectral absolution curve of a set of mixtures with a linear relative increase in the molar concentration of resorufin. The obtained curves with unit normalisation of the pure resazurin peak were rescaled to the absorption value for the experimental solution of pure resazurin typical for biomedical investigations (the mass fraction of pure resazurin in the solution was equal to 0.012%), controlled by the spectral curve obtained in the earlier experiment [23] and converted to the transmittance for the optical path 10 mm typical for a plate's well depth basing on the Beer–Lambert law. The resulting spectral curves were converted to colours using, as an intermediate step, the CIE xyZ colour space, which directly operates with the spectral matching functions. After this, the target colours (see Figure 3A) were obtained by the conversion to the CIE L*a*b* colour space for the lumen level of 100 lm. The obtained dependences on resorufin's concentration for the coordinates a* and b* are shown in Figure 3B.

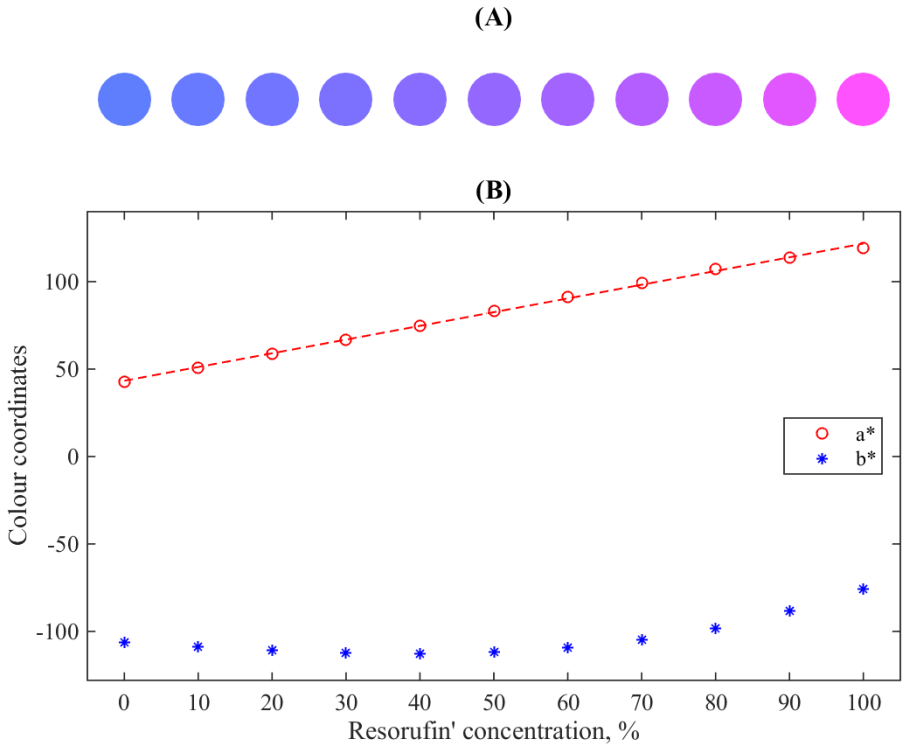

Figure 3. The model colour change due to mixing of resazurin and resorufin with a step of 10% in resorufin's molar concentration (**A**) and the respective change in the CIE L*a*b* colour space coordinates (**B**). The dashed straight line highlights the linear correlation.

One can see that the coordinate b* varies insignificantly except for a not very large elevation in nonlinear deviation for the highest concentrations of resorufin. At the same time, the concentration dependence for the a* coordinate is a practically perfect straight line (the coefficient of determination $R^2 = 0.998$ and the p-value is equal to $3.9 \cdot 10^{-14}$). Thus, this colour coordinate is actually uniformly linearly dependent on the presence of resorufin in a mixture. It is important to note that, although the coordinate values shown in Figure 3B are calculated for a specific lumen level, which is the default for the Osram system (CIE 1931 2° calculated over the range of 360–830 nm), the linear relationship can be expressed in a universal form: $a^*/a^*(0) = 1 + 0.018c_{Rf}$. This equation is independent of the lumen level, where $a^*(0)$ represents the a* coordinate for pure resazurin (i.e., at zero relative concentration of resorufin, c_{Rf}). This representation substantiates the usage of relative units for the analysis of dose–response curves as implemented in the described software.

The conclusions made above on the basis of colorimetric modelling are also supported by comparison with the data on fluorescence (Figure 2C,D): since only resorufin is fluorescent, this coincidence clearly indicates its presence. This stability in relation to non-uniform illumination enables the extraction of quantitative data from images of microbiological plates taken with a standard smartphone, without the need for specialised equipment designed to ensure controlled lighting conditions. Moreover, one can use a variety of plate images published earlier in various research papers for illustrative purposes, but now for quantitative research. This may enrich the content of databases of drug action including exploration of the historical evolution of drug resistance to particular compounds.

The quantitative colorimetric analysis also provides the confirmation that some peculiarities seen in the records of fluorescence actually relate to the change in the indicator medium induced by the activity of microorganisms and not artefacts of the spectrophotometric plate reader. This feature is illustrated in the case of compound 18, where the

growth of fluorescence is seen when the drug concentration exceeds some limit. As seen in Figure 2D, the colorimetric signal is growing under the same conditions too, i.e., there is a transition from blue resazurin to pink resorufin in the respective wells of the plate. Therefore, it is pharmacological (e.g., some kind of generalised hormesis [33]) and not an instrumental effect.

Further, the obtained fitting gives the dose–response curve, which is a more objective measure of the inhibitory action of drugs on a microbial culture. Several modern approaches recommend [15] the usage of the MIC defined as some prescribed inhibitory concentration, e.g., IC_{50}, IC_{90}, and IC_{99} (the particular chosen criterion should be denoted). As mentioned above, the developed approach and software may allow the exploration of wider coverage of results using photographic images without the need for expensive commercial spectrofluorometric plate readers. The development of cost-reducing methods is currently being emphasised as crucial in the context of reducing the public health burden of tuberculosis, particularly in low-income countries where the disease is the most prevalent [34]. These methods are seen as vital for improving accessibility to diagnostic and treatment tools in resource-constrained environments, thus contributing to more effective disease management and control. Active emergence of multi-drug-resistant strains requires massive testing during the curing procedure, carried out at local medical points, where methods of molecular and other hi-tech diagnostics can be inaccessible [35,36]. The combination of easy photographing with the proposed data processing code for open-source software may be a step toward the solution of this problem in situ, as well as using the potential of telemedicine as discussed in a recent review [37].

5. Conclusions and Outlooks

In this work, we provided a computer code, which can be run using open-source software, primarily aimed at quantitative characterisation of the response of a mycobacterial culture to antimycobacterial drugs. It operates by processing digital images, which can be obtained even with a smartphone's camera. It is shown that this approach gives results that are statistically comparable to the results obtained with plate spectrophotometers. At the same time, it has a crucial advantage in the sense of cost and accessibility: the fluorometric plate readers are quite expensive, which makes them unavailable for resource-limited settings, while a smartphone is a common device and ImageJ and GNU Octave are freeware. The main principle of the data processing is based on the usage of single-channel data in the CIE L*a*b* colour system, established with respect to the previous visual spectral changes of the indicator chemicals [23] and to the fluorescence-based data in this work. We would like to draw attention to the fact that the proper choice of the colour space simplified the chemical and biochemical interpretation: the a* channel of the perceptually uniform colour space CIE L*a*b* is robustly linearly proportional to the concentration of the indicator substance, resorufin. Conversely, the perceptually non-uniform, although widespread, RGB requires more complex multichannel calibration, which utilises procedures varying from sophisticated multichannel correlation [18] to machine learning methods [38] and well-controlled conditions of colorimetric recordings [19,20].

At the same time, we have to formulate some caveats, which determine some limitations of the proposed method and application of the developed software. First of all, with regard to the quality of images used for the processing, (i) they should not have significant perspective distortions; otherwise, the rectangular lattice of circles choosing central parts of the microplate's wells will not cover all 96 wells accurately. (ii) Although some deficit and non-uniformity of illumination could be corrected, it is strictly advised to use scattered illumination normally incident to the microplate's surface (also, avoid glares); otherwise, colour reproduction adequacy will be questionable. (iii) When operating with the procession of retrospective imaging data, one should take care that images must not be colour-enhanced.

Finally, let us note that the applicability of the resazurin-based test is not limited by problems of tuberculosis-related studies; it is a wide-purpose reagent for cell viability and cytotoxicity research [14] and recent works denote a widening range of its applications [17,39]. Since the principle of action of the proposed method is based on the basic colorimetric properties of the resazurin–resorufin conversion, it can be applied to a wider range of biophysical systems as well. Moreover, we would like to denote one more prospective application related to the usage of resazurin as a "smart tracer" in environmental hydrological research [40,41]. These studies are unavoidably conducted in field conditions, where one can not take bulky spectrophotometric equipment, but taking pictures with a smartphone with subsequent digital image processing can be carried out easily.

Supplementary Materials: The following supporting information can be downloaded at https://www.mdpi.com/article/10.3390/analytica5040041/s1: the program's code (ColorMICplate.m) and the manual for its usage (manual.pdf); two folders ('compound_16' and 'compound_18') containing the test data.

Author Contributions: Conceptualisation, E.B.P. and A.I.L.; methodology, A.V.S. and E.B.P.; software, E.B.P.; validation, A.V.S. and A.I.L.; formal analysis, E.B.P.; investigation, A.V.S., E.B.P. and A.I.L.; writing—original draft preparation, E.B.P.; writing—review and editing, E.B.P. and A.I.L.; visualisation, E.B.P.; funding acquisition—A.I.L., supervision, E.B.P. and A.I.L. All authors have read and agreed to the published version of the manuscript.

Funding: The mathematical part is supported by the Ministry of Science and Higher Education of the Russian Federation, project 075-02-2023-934; the experimental part is performed within the framework of State Assignment of the Ministry of Health of Russian Federation No. 121112600145-2.

Data Availability Statement: Raw images of microplates used for the reported case studies are free available as a Supplementary Material to the work [25]. The program code and colorimetric data tables are provided as Supplementary Material to this article.

Conflicts of Interest: The authors declare no conflicts of interest.

References

1. Fan, Y.; Li, J.; Guo, Y.; Xie, L.; Zhang, G. Digital image colorimetry on smartphone for chemical analysis: A review. *Measurement* **2021**, *171*, 108829. [CrossRef]
2. Soares, S.; Fernandes, G.M.; Rocha, F.R.P. Smartphone-based digital images in analytical chemistry: Why, when, and how to use. *Trac Trends Anal. Chem.* **2023**, *168* , 117284. [CrossRef]
3. Mitsushio, M. Laboratory-on-a-Smartphone. *Anal. Sci.* **2019**, *36*, 141–142. [CrossRef] [PubMed]
4. Oncescu, V.; O'Dell, D.; Erickson, D. Smartphone based health accessory for colorimetric detection of biomarkers in sweat and saliva. *Lab Chip* **2013**, *13*, 3232–3238. [CrossRef] [PubMed]
5. Giavazzi, F.; Salina, M.; Ceccarello, E.; Ilacqua, A.; Damin, F.; Sola, L.; Chiari, M.; Chini, B.; Cerbino, R.; Bellini, T.; et al. A fast and simple label-free immunoassay based on a smartphone. *Biosens. Bioelectron.* **2014**, *58*, 395–402. [CrossRef]
6. Luo, W.; Deng, J.; He, J.; Han, Z.; Huang, C.; Li, Y.; Fu, Q.; Chen, H. A smartphone-based multi-wavelength photometer for on-site detection of the liquid colorimetric assays for clinical biochemical analyses. *Sensors Actuators Chem.* **2021**, *329*, 129266. [CrossRef]
7. Kap, Ö.; Kılıç, V.; Hardy, J.G.; Horzum, N. Smartphone-based colorimetric detection systems for glucose monitoring in the diagnosis and management of diabetes. *Analyst* **2021**, *146*, 2784–2806. [CrossRef]
8. Hasan, M.K.; Haque, M.; Sakib, N.; Love, R.; Ahamed, S.I. Smartphone-based human hemoglobin level measurement analyzing pixel intensity of a fingertip video on different color spaces. *Smart Health* **2018**, *5–6.* 26–39. [CrossRef]
9. Bergua, J.F.; Alvarez-Diduk, R.; Idili, A.; Parolo, C.; Maymó, M.; Hu, L.; Merkoçi, A. Low-cost, user-friendly, all-integrated smartphone-based microplate reader for optical-based biological and chemical analyses. *Anal. Chem.* **2022**, *94*, 1271–1285. [CrossRef]
10. Chen, J.L.; Miao, Y.; Sun, Q.; Peng, Y.K.; Mao, G.; Dai, W.; Tang, C.; Chen, J. Development of a portable, microwell-based, smartphone-assisted colorimetric device to measure the activities of anaerobic digestion. *Environ. Sci. Adv.* **2024**, *3*, 19–27. [CrossRef]
11. Palomino, J.C.; Martin, A.; Camacho, M.; Guerra, H.; Swings, J.; Portaels, F. Resazurin microtiter assay plate: Simple and inexpensive method for detection of drug resistance in *Mycobacterium tuberculosis*. *Antimicrob. Agents Chemother.* **2002**, *46*, 2720–2722. [CrossRef] [PubMed]

12. Singh, S.; Kumar, P.; Sharma, S.; Mumbowa, F.; Martin, A.; Durier, N. Rapid identification and drug susceptibility testing of *Mycobacterium tuberculosis*: Standard operating procedure for non-commercial assays: Part 3: Colorimetric redox indicator assay v1. 3.12. *J. Lab. Physicians* **2012**, *4*, 120–126. [CrossRef] [PubMed]
13. Rampersad, S.N. Multiple applications of Alamar Blue as an indicator of metabolic function and cellular health in cell viability bioassays. *Sensors* **2012**, *12*, 12347–12360. [CrossRef]
14. Präbst, K.; Engelhardt, H.; Ringgeler, S.; Hübner, H. Basic colorimetric proliferation assays: MTT, WST, and Resazurin. In *Cell Viability Assays: Methods and Protocols*; Gilbert, D.F., Friedrich, O., Eds.; Humana Press: New York, NY, USA, 2017; pp. 1–17. [CrossRef]
15. Franzblau, S.G.; DeGroote, M.A.; Cho, S.H.; Andries, K.; Nuermberger, E.; Orme, I.M.; Mdluli, K.; Angulo-Barturen, I.; Dick, T.; Dartois, V.; et al. Comprehensive analysis of methods used for the evaluation of compounds against *Mycobacterium tuberculosis*. *Tuberculosis* **2012**, *92*, 453–488. [CrossRef]
16. Bento, C.M.; Gomes, M.S.; Silva, T. Evolution of antibacterial drug screening methods: Current prospects for mycobacteria. *Microorganisms* **2021**, *9*, 2562. [CrossRef]
17. Njoku, D.I.; Guo, Q.; Dai, W.; Chen, J.L.; Mao, G.; Sun, Q.; Sun, H.; Peng, Y.K. The multipurpose application of resazurin in micro-analytical techniques: Trends from the microbial, catalysis and single molecule detection assays. *Trac Trends Anal. Chem.* **2023**, *167*, 117288. [CrossRef]
18. Borra, R.C.; Lotufo, M.A.; Gagioti, S.M.; Barros, F.d.M.; Andrade, P.M. A simple method to measure cell viability in proliferation and cytotoxicity assays. *Braz. Oral Res.* **2009**, *23*, 255–262. [CrossRef]
19. Needs, S.H.; Osborn, H.M.I.; Edwards, A.D. Counting bacteria in microfluidic devices: Smartphone compatible 'dip-and-test' viable cell quantitation using resazurin amplified detection in microliter capillary arrays. *J. Microbiol. Methods* **2021**, *187*, 106199. [CrossRef] [PubMed]
20. de Santana, P.C.; Lourenco, F.R. A smartphone-based bioassay for determining relative potency estimated from sigmoidal-response curves and respective measurement uncertainty. *Microchem. J.* **2020**, *154*, 104626. [CrossRef]
21. Malacara, D. *Color Vision and Colorimetry: Theory and Applications*; SPIE: Bellingham, WA, USA, 2011.
22. Fernandes, G.M.; Silva, W.R.; Barreto, D.N.; Lamarca, R.S.; Gomes, P.C.F.L.; da S Petruci, J.F.; Batista, A.D. Novel approaches for colorimetric measurements in analytical chemistry—A review. *Anal. Chim. Acta* **2020**, *1135*, 187–203. [CrossRef]
23. Sychev, A.V.; Lavrova, A.I.; Dogonadze, M.Z.; Postnikov, E.B. Establishing Compliance between Spectral, Colourimetric and Photometric Indicators in Resazurin Reduction Test. *Bioengineering* **2023**, *10*, 962. [CrossRef] [PubMed]
24. Krasavin, M.; Parchinsky, V.; Kantin, G.; Manicheva, O.; Dogonadze, M.; Vinogradova, T.; Karge, B.; Brönstrup, M. New nitrofurans amenable by isocyanide multicomponent chemistry are active against multidrug-resistant and poly-resistant *Mycobacterium tuberculosis*. *Bioorganic Med. Chem.* **2017**, *25*, 1867–1874. [CrossRef] [PubMed]
25. Krasavin, M.; Mujumdar, P.; Parchinsky, V.; Vinogradova, T.; Manicheva, O.; Dogonadze, M. Library of diversely substituted 2-(quinolin-4-yl) imidazolines delivers novel non-cytotoxic antitubercular leads. *J. Enzym. Inhib. Med. Chem.* **2016**, *31*, 1146–1155. [CrossRef]
26. Postnikov, E.B.; Lavrova, A.I. Statistical features of REMA data of antimycobacterial drug screening and determining the minimal inhibitory concentration. In Proceedings of the 2021 6th International Conference on Intelligent Informatics and Biomedical Sciences (ICIIBMS), Oita, Japan, 25–27 November 2021 ; IEEE: Piscataway, NJ, USA, 2021; Volume 6, pp. 107–108. [CrossRef]
27. Sternberg, S.R. Biomedical Image Processing. *Computer* **1983**, *16*, 22–34. [CrossRef]
28. Angelani, C.R.; Carabias, P.; Cruz, K.M.; Delfino, J.M.; de Sautu, M.; Espelt, M.V.; Ferreira-Gomes, M.S.; Gómez, G.E.; Mangialavori, I.C.; Manzi, M.; et al. A metabolic control analysis approach to introduce the study of systems in biochemistry: The glycolytic pathway in the red blood cell. *Biochem. Mol. Biol. Educ.* **2018**, *46*, 502–515. [CrossRef]
29. Analytical Methods Committee. Robust statistics: A method of coping with outliers. In *Amc Technical Brief*; No. 6; Analytical Methods Committee: Cambridge, UK, 2001.
30. Motulsky, H.; Christopoulos, A. *Fitting Models to Biological Data Using Linear and Nonlinear Regression: A Practical Guide to Curve Fitting*; Oxford University Press: Oxford, UK, 2004.
31. AAT Bioquest. Absorption Spectrum Viewer. Available online: https://www.aatbio.com/absorbance-uv-visible-spectrum-graph-viewer/resazurin (accessed on 9 August 2024).
32. AAT Bioquest. Absorption Spectrum Viewer. Available online: https://www.aatbio.com/absorbance-uv-visible-spectrum-graph-viewer/resorufin (accessed on 9 August 2024).
33. Kendig, E.L.; Le, H.H.; Belcher, S.M. Defining hormesis: Evaluation of a complex concentration response phenomenon. *Int. J. Toxicol.* **2010**, *29*, 235–246. [CrossRef] [PubMed]
34. Siapka, M.; Vassall, A.; Cunnama, L.; Pineda, C.; Cerecero, D.; Sweeney, S.; Bautista-Arredondo, S.; Bollinger, L.; Cameron, D.; Levin, C.; et al. Cost of tuberculosis treatment in low-and middle-income countries: Systematic review and meta-regression. *Int. J. Tuberc. Lung Dis.* **2020**, *24*, 802–810. [CrossRef]
35. Fisher, M. Diagnosis of MDR-TB: A developing world problem on a developed world budget. *Expert Rev. Mol. Diagn.* **2002**, *2*, 151–159. [CrossRef] [PubMed]
36. Groessl, E.J.; Ganiats, T.G.; Hillery, N.; Trollip, A.; Jackson, R.L.; Catanzaro, D.G.; Rodwell, T.C.; Garfein, R.S.; Rodrigues, C.; Crudu, V.; et al. Cost analysis of rapid diagnostics for drug-resistant tuberculosis. *BMC Infect. Dis.* **2018**, *18*, 102. [CrossRef]

37. Olawade, D.B.; Eberhardt, J.; David-Olawade, A.C.; Balogun, M.A.; Bolarinwa, O.A.; Esan, D.T. Transforming multidrug-resistant tuberculosis care: The potentials of telemedicine in resource-limited settings. *Health Sci. Rev.* **2024**, *12*, 100185. [CrossRef]
38. Thanasirikul, C.; Patumvan, A.; Lipsky, D.; Bovonsombut, S.; Singjai, P.; Boonchieng, E.; Chitov, T. Rapid assessment and prediction of microbiological quality of raw milk using machine learning based on RGB-colourimetric resazurin assay. *Int. Dairy J.* **2023**, *146*, 105750. [CrossRef]
39. Lavogina, D.; Lust, H.; Tahk, M.J.; Laasfeld, T.; Vellama, H.; Nasirova, N.; Vardja, M.; Eskla, K.L.; Salumets, A.; Rinken, A.; et al. Revisiting the Resazurin-Based Sensing of Cellular Viability: Widening the Application Horizon. *Biosensors* **2022**, *12*, 196. [CrossRef] [PubMed]
40. Knapp, J.L.A.; González-Pinzón, R.; Haggerty, R. The resazurin-resorufin system: Insights from a decade of "smart" tracer development for hydrologic applications. *Water Resour. Res.* **2018**, *54*, 6877–6889. [CrossRef]
41. Ma, R.; Chen, K.; Andrews, C.B.; Loheide, S.P.; Sawyer, A.H.; Jiang, X.; Briggs, M.A.; Cook, P.G.; Gorelick, S.M.; Prommer, H.; et al. Methods for quantifying interactions between groundwater and surface water. *Annu. Rev. Environ. Resour.* **2024**, *49*, 623–653. [CrossRef]